Published online June 2, 2005

Nucleic Acids Research, 2005, Vol. 33, No. 10 ***3133–3144***
doi:10.1093/nar/gki630

Reconstitution of archaeal H/ACA small ribonucleoprotein complexes active in pseudouridylation

Bruno Charpentier*, Sébastien Muller and Christiane Branlant

Laboratoire de Maturation des ARN et Enzymologie Moléculaire, UMR 7567 UHP-CNRS, Université des Sciences et Techniques Henri Poincaré Nancy I, 54506 Vandoeuvre-Lès-Nancy cedex, France

Received April 26, 2005; Revised and Accepted May 15, 2005

ABSTRACT

Pseudouridine (Ψ) are frequently modified residues in RNA. In Eukarya, their formation is catalyzed by enzymes or by ribonucleoprotein complexes (RNPs) containing H/ACA snoRNAs. H/ACA sRNA and putative ORFs for H/ACA sRNP proteins (L7Ae, aCBF5, aNOP10 and aGAR1) were found in Archaea. Here, by using *Pyrococcus abyssi* recombinant proteins and an *in vitro* transcribed *P.abyssi* H/ACA sRNA, we obtained the first complete *in vitro* reconstitution of an active H/ACA RNP. Both L7Ae and the aCBF5 RNA:Ψ synthase bind directly the sRNA; aCBF5 also interacts directly and independently with aNOP10 and aGAR1. Presence of aCBF5, aNOP10 and a U residue at the pseudouridylation site in the target RNA are required for RNA target recruitment. In agreement, we found that the aCBF5–aNOP10 pair is the minimal set of proteins needed for the formation of a particle active for pseudouridylation. However, particles more efficient in targeted pseudouridylation can be formed with the addition of proteins L7Ae and/or aGAR1. Although necessary for optimal activity, the conserved ACA motif in the sRNA was found to be not essential.

INTRODUCTION

Conversion of uridines into pseudouridines (Ψ) and riboses 2′-O-methylation are the two most frequent RNA post-transcriptional modifications [for review, (1,2)]. Some of these modifications are highly important for the activity of RNAs in translation or pre-mRNA splicing (3–7). In Eukarya and Archaea, both modifications can be generated by two distinct systems. Either a single protein has the specific RNA modification activity: RNA:Ψ-synthase [for review, (8)] or RNA:2′-O-methylase activity [for review, (9)]; or the proteins carrying these enzymatic activities are found within ribonucleoprotein complexes (RNP) containing small RNAs. These RNAs are designated as small nucleolar RNAs (snoRNAs) in Eukarya and sRNAs in Archaea. They define the positions to be modified by base-pair interaction with the targeted RNAs [for review, (10–13)]. Based on conserved structural features, the snoRNAs and sRNAs can be divided into two classes: RNAs with C and D boxes (eukaryal C/D snoRNAs and archaeal C/D sRNAs) that guide 2′-O-methylations (14,15), and RNAs with H/ACA boxes (eukaryal H/ACA snoRNAs and archaeal H/ACA sRNAs) that guide RNA pseudouridylations (16,17). Among the proteins associated with C/D box RNAs, the Snu13p/15.5 kDa protein in Eukarya and its L7Ae archaeal counterpart play an essential role in the initiation of RNP assembly (18–20). C/D sRNPs active in 2′-O-methylation have already been reconstituted from *in vitro* transcribed RNAs and recombinant proteins (18,21–24). Interestingly, the archaeal L7Ae protein is also able to bind the H/ACA sRNAs (25). However, limited information is available on the H/ACA sRNP assembly and function.

Information on H/ACA RNPs largely comes from eukaryal H/ACA snoRNP analyses. All H/ACA snoRNAs contain two irregular hairpin structures linked by a hinge sequence and followed by a short 3′ tail. The ANANNA sequence (Box H) present in the hinge region and the ACA sequence (Box ACA), which is located three nucleotides upstream of the RNA 3′ end, are essential for snoRNA stability and function (16,26,27). Each of the hairpin structures contains a central loop that carries a 9–13 bp bipartite antisense element. After hybridization of this loop with the target RNA, a pseudouridylation pocket is formed. In this structure, an unpaired dinucleotide of the target RNA is surrounded by two short bimolecular helices; it contains the U residue converted into a Ψ residue (17,28). Genetic data in yeast, as well as biochemical analysis of purified H/ACA snoRNPs, provided strong evidence for the presence of an evolutionarily conserved RNA:Ψ-synthase in H/ACA snoRNPs (Cbf5p in yeast, dyskerin or NAP57 in

*To whom correspondence should be addressed. Tel: +33 3 83 68 43 16; Fax: +33 3 83 68 43 07; Email: bruno.charpentier@maem.uhp-nancy.fr

human) (29–31). H/ACA snoRNPs contain three other core proteins (denoted Nhp2p, Nop10p and Gar1p in yeast, and NHP2, NOP10 and GAR1 in human) (32,33). Active H/ACA snoRNPs were immunopurified from HeLa cell extracts (34). By mild denaturing treatment of yeast H/ACA snoRNPs, a complex formed by proteins Cbf5p, Gar1p and Nop10p was obtained, showing the occurrence of protein–protein interaction in the RNPs (35). Recently, assays for assembly of mammalian H/ACA snoRNPs were performed using proteins produced by *in vitro* transcription/translation (36). In accordance with previous data obtained by immunoprecipitation experiments and *in vitro* reconstitution of H/ACA snoRNP in cellular extract (37,38), the authors demonstrated that the NOP10–NAP57 interaction is a prerequisite for NHP2 binding and that the NAP57–NOP10–NHP2 core trimer specifically recognizes H/ACA snoRNAs (36). In spite of these progresses in understanding how H/ACA snoRNP components interact together, up to now, functional H/ACA snoRNPs could only be obtained by incubation of a snoRNA transcript with a cytosolic extract (34,36).

Based on the successful reconstitution of active archaeal C/D sRNPs using *in vitro* transcribed RNA and recombinant proteins, we tested the possibility to reconstitute archaeal H/ACA sRNPs from recombinant molecules. Three H/ACA sRNAs have recently been identified in the hyperthermophile archaeon *Archaeoglobus fulgidus* (39). The secondary structures of these RNAs are quite less homogeneous than those of eukaryal H/ACA snoRNAs. They are folded into one, two or three stem–loop structures, each containing a pseudouridylation pocket (39). In addition, they all exhibit a sequence able to form a terminal pseudo K-turn motif recognized by the protein L7Ae (25,40,41). Protein L7Ae is proposed to have a common ancestor with the eukaryal Snu13p/15.5 kDa and Nhp2 proteins (20,33,42). In addition, based on DNA sequence analysis, homologues of the eukaryal Cbf5, Nop10 and Gar1 proteins were expected to be present in archaea (38,42). However, their interactions with H/ACA sRNAs have not been demonstrated.

Here, we report the reconstitution of a *Pyrococcus abyssi* pseudouridylation-competent particle by incubation of an *in vitro* transcribed H/ACA sRNA with the four recombinant archaeal L7Ae, aCBF5, aNOP10 and aGAR1 proteins. RNA–protein interactions were analyzed by gel retardation assays. An optimal guided pseudouridylation activity was obtained in the presence of the four core proteins. However, particles assembled in the absence of aGAR1 can specifically modify, albeit less rapidly, an RNA substrate. As it was the case for C/D sRNPs, the development of conditions for *in vitro* reconstitution of active H/ACA sRNPs is expected to open the door for further investigation on the architecture and the mechanism of action of these particles.

MATERIALS AND METHODS

Oligonucleotides

Pairs of primers used for PCR amplification of *P.abyssi* open reading frames (ORFs) and DNA templates for T7 *in vitro* transcription of Pab91 sRNA, and for site-directed mutagenesis can be obtained upon request (see also Supplementary Material).

Recombinant protein production

The ORFs of archaeal L7Ae, aNOP10, aGAR1 and aCBF5 proteins (GenBank accession nos C75109, CAB49761, CAB49230 and CAB49444, respectively) were PCR-amplified from the genomic DNA of the *Pyrococcus abyssi* GE5 strain. They were cloned in plasmid pGEX-6P-1 (Pharmacia) to produce GST fusion protein. A multi-step PCR strategy was used to generate the (Asp-82 → Ala, GAC → GCC) site-specific mutation in the aCBF5 domain II.

The recombinant GST-L7Ae, GST-aNOP10, GST-aGAR1, GST-aCBF5 and GST-aCBF5/D82A proteins were produced in *E.coli* BL21 CodonPlus cells (Novagen) and purified under native conditions using Glutathione-Sepharose 4B (Pharmacia) as previously described (43). The fusion proteins were cleaved on beads with 80 U of PreScission protease (Pharmacia) per ml of Glutathione-Sepharose bead suspension. Cleavage was performed overnight at 4°C followed by incubation at 65°C during 15 min. The precipitated contaminant proteins were eliminated by a 20 min centrifugation at 16 000 *g*. For their use in the GST pull-down experiments, the GST-fusion proteins were eluted from the beads by incubation with reduced glutathione following the manufacturer recommendations, and the reduced glutathione was subsequently exchanged with the PBS buffer by loading the eluted proteins on Econo-Pac 10DG columns (Biorad). The quality of protein preparations was assessed by SDS–PAGE and Coomassie staining.

In vitro binding assays

Purified GST or GST-fusion proteins were bound to Glutathione-Sepharose beads in PBS buffer. Recombinant proteins (1 μg each) were incubated for 1 h at 25°C with 15 μl of beads in 100 μl of PBS buffer containing 500 mM NaCl. Bound proteins were washed three times with PBS/NaCl buffer and eluted by boiling in Laemmli loading buffer. After SDS–PAGE, proteins were visualized by Coomassie Blue staining.

DNA templates used for *in vitro* transcription

The Pab91 sRNA sequence was PCR-amplified from the *Pyrococcus abyssi* GE5 genomic DNA using a forward primer containing the T7 RNA polymerase promoter. The DNA templates for production of the Pab91mtKT, Pab91mtACA and Pab91mtKTmtACA variant sRNAs were produced by PCR amplification. Before use, all the PCR amplification products were cloned in the pTAdv vector (Clontech) and their sequences were checked by dideoxynucleotide sequencing.

In vitro transcription of guide and target RNAs

The WT and variant Pab91 sRNAs, and the target RNAs, were *in vitro* transcribed by T7 RNA polymerase using PCR amplification fragments. They were purified by gel electrophoresis. For production of cold RNAs, transcription reactions were carried out as previously described (44). The same conditions were used for synthesis of uniformly labeled RNAs, except that the reaction was performed with 20 μCi of [α-^{32}P]CTP (800 Ci/mmol) (Amersham), 4 mM each of ATP, UTP and GTP, and 0.13 mM CTP. Subsequent RNA treatments were as previously described (45).

Electrophoresis mobility shift assays (EMSA)

About 50 fmol of uniformly ^{32}P-labeled RNA were mixed with 1 μg of yeast tRNA (Roche) in 3.5 μl of buffer D (150 mM KCl, 1.5 mM $MgCl_2$, 0.2 mM EDTA and 20 mM HEPES, pH 7.9). For competition experiments increasing amounts of cold competitor sRNA were added. To study the sRNP-target RNA association, unlabelled RNA-S (2.4 pmol in most experiments or more as indicated in the figures) was added at this stage. Except for K_d determinations, each recombinant proteins was used at a 200 nM concentration and the mixture (4.5 μl final volume in buffer D) was incubated for 10 min at 65 or 20°C. RNA–protein complexes were resolved at room temperature in 6% Triborate non-denaturing polyacrylamide gels, as previously described (44). The dried gels were analyzed with a phosphorimager (Typhoon 9410, Amersham Biosciences) and the amounts of radioactivity in the bands were estimated with the ImageQuant software. The percentage of RNA in each RNP was calculated from the radioactivity in each band relative to the total radioactivity in the lane.

In vitro sRNP guide pseudouridylation assay

Unlabeled sRNA (4 pmol, ~800 nM) and [α-^{32}P]CTP-labeled target RNA-S or RNA-L (150 fmol, ~30 nM) were mixed at room temperature in buffer D and treated as described for EMSA assays. The proteins (200 nM each) were added at room temperature; the final 4.5 μl solution was incubated at 65 or 20°C. For time course experiments, first, the reaction volume was scaled up to 50 μl, using the same RNA and protein concentrations, second, the reaction was started by addition of the proteins after incubation of the RNA solution at 65°C for 10 min. At time intervals, 4.5 μl aliquots were collected. For each aliquot, the reaction was stopped by addition of 150 μl of H_2O and 150 μl of a phenol:chloroform (1:1) mix. The extracted RNAs were ethanol-precipitated. The modified RNA targets were totally digested with 0.5 U of T2 RNase (GibcoBRL) for 12 h at 37°C. The resulting 3′-mononucleotides were chromatographed on thin-layer cellulose plates as described elsewhere (46,47). For reaction performed on the RNA-S, one dimension chromatography was sufficient to fractionate the three labeled 3′-mononucleotides (Figure S1). The radioactivity in the spots or the bands were quantified with a phosphorimager (Amersham Biosciences) using the ImageQuant software. Taking into account the total number of U residues in the target RNA, we determined the amount of Ψ formed (expressed in moles per mole of target RNA).

RESULTS

Proteins L7Ae and aCBF5 bind directly to the Pab91 sRNA

By using computer analysis, we searched for the presence of H/ACA sRNAs in the *Pyrococcus* genera and found in *P.abyssi* a small H/ACA sRNA, which we denoted as Pab91 (Muller, S., Leclerc, F., Behm-Ansmant, I., Charpentier, B. and Branlant, C., in preparation). Its counterpart in *A.fulgidus* is the recently identified Afu46 sRNA (39). We showed that sRNA Pab91 directs pseudouridylation at position 2685 in the *P.abyssi* 23S rRNA (Muller, S., Leclerc, F., Behm-Ansmant, I., Charpentier, B. and Branlant, C., in preparation). The secondary structures of *P.abyssi* Pab91 and *A.fulgidus* Afu46 sRNAs consist of a single stem–loop structure (Figure 1A). It is closed by an L7Ae binding site, which consists of two A•G and G•A sheared pairs, linked by a 4 nt long terminal loop with a 3′ terminal U residue (20,25,39). The Pab91 stem–loop structure is flanked by a short 3′ sequence containing the conserved ACA triplet (Figure 1A). We chose this simple sRNA molecule as a model to develop conditions for *in vitro* reconstitution of archaeal H/ACA sRNPs. The Pab91 sRNA and its variants were synthesized by *in vitro* transcription and the four core proteins aCBF5, aNOP10, aGAR1 and L7Ae were produced as recombinant proteins in *E.coli* and purified.

Except for protein L7Ae, nothing was known on the individual RNA binding capacity of the archaeal H/ACA core proteins, thus, we first tested their direct binding on the WT Pab91 sRNA. Incubation was performed at 65°C, in the presence of 150 mM KCl and a yeast tRNA mixture in excess was used as the competitor (see Materials and Methods). The resulting complexes were analyzed by electrophoresis mobility-shift assays (EMSA) performed at room temperature (Figure 1B). The WT Pab91 sRNA was totally shifted into an RNP1 complex by incubation with protein L7Ae at a 200 nM concentration. In accordance with previous data on the *A.fulgidus* Afu46 sRNA (25), an estimated K_d of ~100 nM was found for complex RNP1 (Figure 1C). As expected from the present knowledge on the determinants required for L7Ae/Snu13p binding on the K-turn structures (22,25,40,41), no binding of protein L7Ae was observed after disruption of the two A•G and G•A sheared pairs in the L7Ae recognition motif (sRNA variant Pab91mtGA, Figures 1A and 2D). In contrast, the ACA triplet was not required for L7Ae binding (sRNA variant Pab91mtACA, Figures 1A and 2C). Concerning the three other proteins, only aCBF5 led to the formation of an RNP complex (RNP2 in Figure 1B). However, even at high aCBF5 protein concentration, its yield of formation was low (Figure 1C). We thus tested the specificity of this interaction by competition experiments using as the competitor, WT or variant Pab91 sRNAs (Figure 1D and E). As the Pab91mtACA sRNA, with a UGU triplet instead of the ACA triplet (i) did not compete formation of RNP2 by the WT sRNA, and (ii) was not able to form an RNP2 complex (Figure 2C), we concluded that the presence of the ACA box is required for aCBF5 binding on the Pab91 sRNA. In contrast, formation of RNP2 with the Pab91mtGA variant sRNA (Figure 2D) showed that an intact L7Ae binding site is not required for RNP2 formation. Hence, in the conditions used, only protein L7Ae and to a lesser extent protein aCBF5 interact directly with the Pab91 sRNA, in addition, aCBF5 binding depends upon the presence of the ACA motif.

Protein aCBF5 but not L7Ae favors protein aNOP10 recruitment

As binding of protein L7Ae strongly favors C/D sRNP assembly (18), we tested whether it could increase aCBF5 binding on a H/ACA sRNA. When the two proteins were incubated with the WT Pab91 sRNA, a second complex (RNP3) was detected in addition to RNP1 (Figure 2A). According to its electrophoretic mobility, it contained both L7Ae and aCBF5. As found for RNP2, RNP3 was obtained in low yield compared to RNP1. However, the yield of RNP3 formation was higher than that of

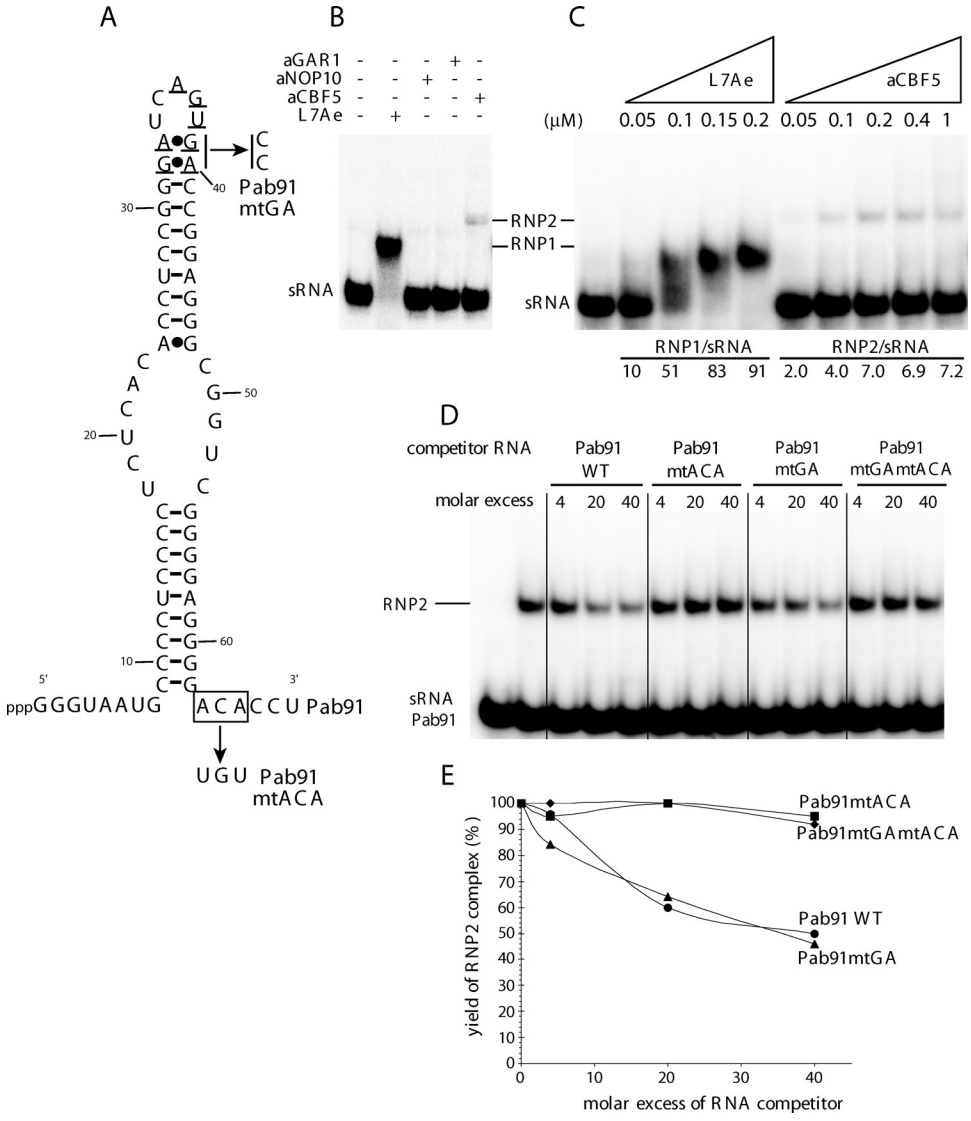

Figure 1. Both L7Ae and aCBF5 bind directly the Pab91 sRNA. (**A**) Secondary structure model of the Pab91 sRNA, folded according to the structure proposed for its counterpart Afu46 sRNA in *A.fulgidus* (39). The ACA motif is boxed, residues of the L7Ae binding site are underlined. The GA to CC and ACA to UGU substitutions in variants Pab91mtGA, Pab91mtACA and Pab91mtGAmtACA are shown. (**B**–**D**) Test of the individual binding of the core proteins by EMSA. *In vitro* transcribed ^{32}P-labeled WT Pab91 sRNA (50 fmol) (Panels B and C), or a mix of labeled WT RNA (50 fmol) and competitor unlabeled WT or variant Pab91 sRNA (0.2, 1 or 2 pmol, corresponding to 4, 20 and 40 molar excess, respectively) (Panel D) were incubated at 65°C with one of the L7Ae, aNOP10, aGAR1 or aCBF5 proteins (200 nM each in panels B and at concentrations increasing from 0.05 to 1 μM in panel C) or with protein aCBF5 (200 nM in panel D). The RNP complexes formed were resolved by electrophoresis at room temperature on native 6% polyacrylamide gels and visualized by exposure to Phosphorimager screens. Positions of the RNA/protein complexes (RNP1 and RNP2) and the free sRNA are indicated. The RNP yields (given below each lane in panel C) were expressed as the percentage of Pab91 sRNA in RNP1 or RNP2 as estimated by radioactivity measurement. The gel in panel D was exposed for a longer time as compared to the ones in panels B and C. (**E**) The RNP2 yields in the gel of panel D were estimated as in panel C. The values were expressed as a percentage of the RNP2 yield formed with the WT Pab91 sRNA in absence of competitor RNA (value of 100%). The values were plotted against the molar excess of cold competitor RNAs.

RNP2 (Figure 2A), the mean value for three different experiments was of 7.5 ± 1.5 for RNP2 and of 16.6 ± 1.3 for RNP3. Hence, the presence of protein L7Ae may have slightly increased aCBF5 association with the RNA. Whereas only RNP1 was formed in the presence of the two L7Ae and aNOP10 proteins (Figure 2A), an RNP4 complex was formed with the aCBF5–aNOP10 protein pair, RNP4 had a lower mobility compared to RNP2 (Figure 2A). Hence, protein aCBF5, but not L7Ae, allows the recruitment of protein aNOP10.

Incubation of the sRNA in the presence of the three L7Ae, aCBF5 and aNOP10 proteins (Figure 2B) led to the formation of a larger RNP5 complex that was expected to contain the three proteins. However, the large amount of residual RNP1 complex reflected a partial association of proteins aNOP10 and aCBF5 with the L7Ae/sRNA complex. The absence of RNP3 complex suggested either the rapid association of protein aNOP10 after binding of protein aCBF5 or the association of a complex formed by these two proteins. Binding of protein aCBF5 was probably a limiting step in our *in vitro* reconstitution experiments. These assumptions are in agreement with our observation of similar RNA-sequence requirements for binding of aNOP10 and aCBF5: namely, the necessity of the ACA motif, but not of the two A•G and G•A sheared-pairs (Figure 2C and D). Accordingly, no RNP4 was formed when

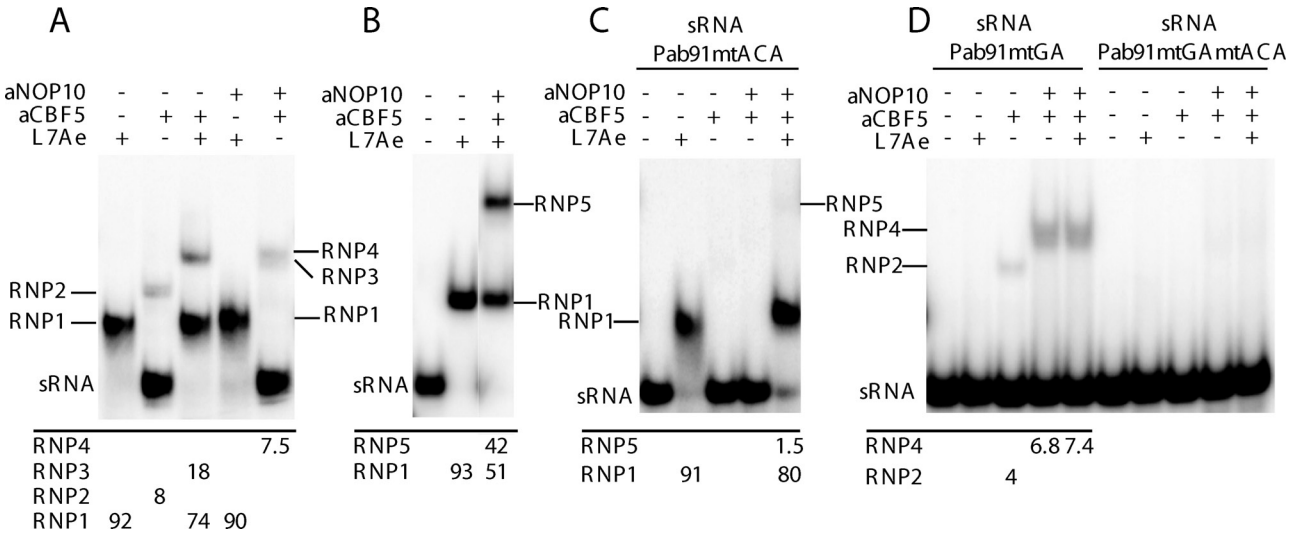

Figure 2. aCBF5 is required for aNOP10 association and association of both proteins depends upon the ACA sequence. (**A** and **B**) Identification by EMSA of the RNP complexes formed with the radiolabeled WT Pab91 sRNA (50 fmol) and various combinations of the core proteins (200 nM each). Incubation was at 65°C. The names of RNPs revealed by phosphorimager analysis are indicated. The percentage of sRNA present in each RNP as referred to the total RNA amount is indicated below each lane. (**C** and **D**) The same experiments as in panels A and B were repeated with the variant Pab91mtACA sRNA (Panel C), Pab91mtGA (Panel D) and Pab91mtGAmtACA (Panel D) sRNAs.

the Pab91mtACA sRNA variant was incubated with proteins aNOP10 and aCBF5 (Figure 2C), whereas both RNP2 and RNP4 complexes were formed with the Pab91mtGA sRNA variant (Figure 2D). Only a very low amount of RNP5 was detected upon incubation of the Pab91mtACA sRNA with the aNOP10, aCBF5 and L7Ae proteins (Figure 2C).

To test for a possible interaction between aCBF5 and aNOP10, we coated the GST-aNOP10 fusion protein on Glutathione-Sepharose beads and tested whether protein aCBF5 binds to these beads in the presence of 500 mM NaCl. As shown by SDS–PAGE analysis, protein aCBF5 but not L7Ae was retained (Figure 3). As aCBF5 was not retained in the control experiment performed with the GST alone, we concluded that aCBF5 and aNOP10 can interact together, and the interaction is stable even at high salt concentration.

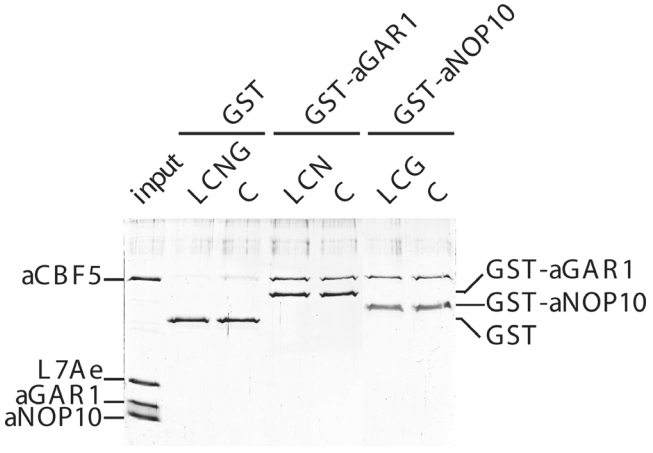

Figure 3. The GST-aNOP10 and GST-aGAR1 fusion proteins bind aCBF5 *in vitro*. Different combinations (as indicated above each lanes) of purified recombinant proteins aCBF5 (C), aNOP10 (N), aGAR1 (G) and L7Ae (L) were incubated in buffer containing 500 mM NaCl in the presence of Glutathione-Sepharose beads coated with the GST, GST-aGAR1 or GST-aNOP10 proteins. The bound proteins were fractionated by SDS–PAGE and stained by Coomassie blue.

Presence of the three aCBF5, aNOP10 and L7Ae proteins is required for efficient association of an RNA substrate

Next, we investigated whether the identified RNP complexes can interact with an RNA substrate. We produced a 22 nt long RNA substrate (RNA-S, Figure 4A), carrying the *P.abyssi* 23S rRNA fragment extending from positions 2673 to 2692, that is targeted by the Pab91 sRNA (Muller, S., Leclerc, F., Behm-Ansmant, I., Charpentier, B. and Branlant, C., in preparation). By using an unlabeled RNA-S target and a labeled sRNA, we first verified that, in the absence of protein and in the buffer and temperature conditions used for complex assembly, no stable interaction takes place between the radiolabeled guide sRNA and the targeted RNA (Figure 4B, lane 1). Then, we tested whether the presence of the RNA substrate was altering the electrophoretic mobility of complexes formed by incubation of the WT sRNA with various combinations of the H/ACA sRNP proteins, at 20 or 65°C. When proteins L7Ae and aCBF5 were incubated individually with the sRNA, addition of the RNA target did not modify significantly the yield and electrophoretic mobilities of RNP1 and RNP2 (Figure 4B). In contrast, addition of the RNA target upon incubation of the WT sRNA with the aCBF5–aNOP10 protein pair, increased the yield of RNP formation (Figure 4C, lanes 2–5). The RNP4/RNA-S complex obtained was designated as complex CI. The differences in the percentages of sRNAs in RNP4 and CI in three distinct experiments are significant as judged by a $P < 0.01$ measured by a Student's paired *t*-test. In addition, the RNP1 and RNP5 complexes detected upon incubation of the guide RNA with the three L7Ae, aCBF5 and aNOP10 proteins were almost completely

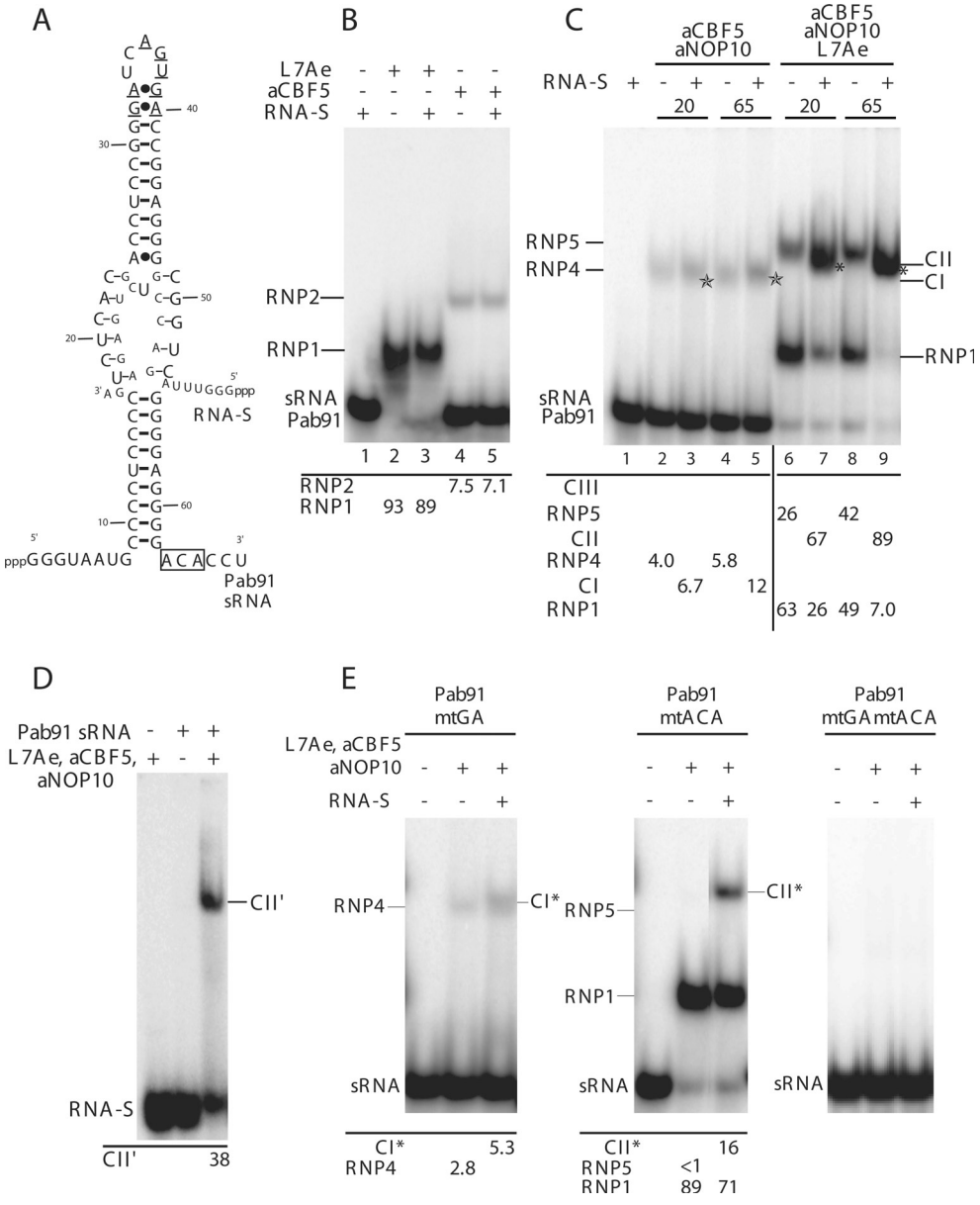

Figure 4. Presence of the target RNA favors sRNP assembly *in vitro*. (**A**) Model of the interaction between the Pab91 sRNA and the RNA-S target. The U residue converted into a Ψ residue is in bold. (**B** and **C**) Identification by gel shift assays of complexes formed with a radiolabeled WT Pab91 sRNA (50 fmol) and various combinations of the core proteins (200 nM each), in the presence or absence of a 50 molar excess of unlabeled target RNA-S (as indicated above the lanes). Incubation was at 65°C in panel B, and 20 or 65°C in panel C. The names of RNP complexes identified by phosporimager analysis are indicated, as well as the percentage of Pab91 sRNA in each complex. (**D**) Same experiment as in lane 9 of panel C, except that RNA-S was the radiolabeled RNA (150 fmol) and that 2 pmol of unlabeled Pab91 sRNA were used. (**E**) The RNA-S target stabilizes sRNP complex formation with the variant Pab91mtGA and Pab91mtACA sRNAs. Similar experiments as in panel C, lanes 8 and 9, were performed with the three variant Pab91 sRNAs.

converted into a unique CII complex in the presence of the RNA substrate (Figure 4C, lanes 6–9). Complex CII had an electrophoretic mobility higher than that of RNP5. The yield of complex CII formation was slightly higher at 65°C compared to 20°C. To verify the incorporation of the RNA substrate into the CII complex, the same experiment was repeated using an unlabeled guide sRNA and a radiolabeled RNA-S target. As expected, a large part of the RNA substrate was shifted into a CII′ complex, which had an electrophoretic mobility similar to that of complex CII and is expected to be identical (Figure 4D). Altogether, the data suggested an efficient binding of the RNA substrate on the RNP complex when protein aNOP10 was present in this complex.

Presence of a uridine at the isomerization site reinforces the yield of complex CII formation

To test for the specificity of the RNA target selection by RNP5, we incubated the WT radiolabeled sRNA with the L7Ae, aCBF5 and aNOP10 proteins, in the presence of increasing amounts of the WT RNA substrate (RNA-S) or a variant RNA substrate (RNA-S-mtU). This variant RNA had a U to

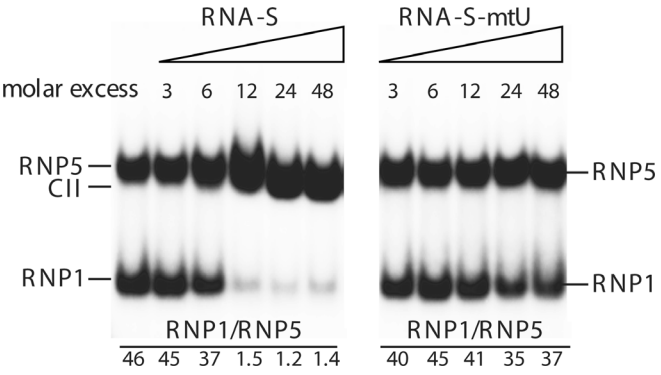

Figure 5. The targeted U residue is required for stable sRNP/RNA-S complex formation. Incubations was as in Figure 4C, lane 9, except that the WT (RNA-S) or mutated (RNA-S-mtU) target RNA was used at concentrations varying from 22 to 530 nM (molar excess from 3 to 48, as indicated above the lanes). The percentages of Pab91 sRNA in RNP5 and complex CII are given below the lanes.

C substitution at the isomerization site. Interestingly, whereas in the presence of 0.6 pmol of RNA-S (12-fold molar excess), almost all the guide sRNA was found in complex CII (Figure 5), a large part of the RNP1 was not displaced into complex CII when the same experiment was performed with RNA-S-mtU. Even at a 48-fold molar excess of RNA-S-mtU, RNP1 was still detected (Figure 5). This strongly suggests that the occurrence of a U residue at the isomerization site is important for efficient formation of a stable sRNP/RNA-S complex.

Binding of the targeted RNA requires at least one of the two sRNA conserved motifs

As RNP4 can be formed with the Pab91mtGA variant sRNA and as RNP5 was detected in trace amounts with the Pab91mtACA variant sRNA (Figure 2), we tested whether the RNA-S target can associate with these RNPs. As shown in Figure 4E, a CI-like complex (CI*), similar to the CI complex obtained with the WT sRNA, was formed with the Pab91mtGA variant and a CII-like complex (CII*) was also obtained with the Pab91mtACAvariant. The yield of CII* formation was lower (16%) compared to that of CII (89%). However, taking into account the very low level of RNP5 formation on the Pab91mtACA variant in the absence of RNA substrate, this latter strongly reinforces complex formation on the Pab91mtACA variant sRNA. The positive effect of substrate addition is not observed in the double mutant (sRNA variant Pab91mtGAmtACA, Figure 4E).

A negative effect of protein aGAR1 on RNP assembly is counteracted by the RNA target

Surprisingly, incubation of the WT Pab91 sRNA with proteins aCBF5 and aGAR1 revealed a negative effect of protein aGAR1 on RNP2 formation (Figure 6B). In addition, in the presence of aGAR1, no large RNP complex was detected when the three L7Ae, aCBF5 and aNOP10 proteins were incubated with the sRNA (Figure 6C). Even the RNP1 complex was found in lower yields in these conditions. Thus, in the incubation conditions used, protein aGAR1 had either a negative effect on protein assembly or a destabilization effect on the complex formed.

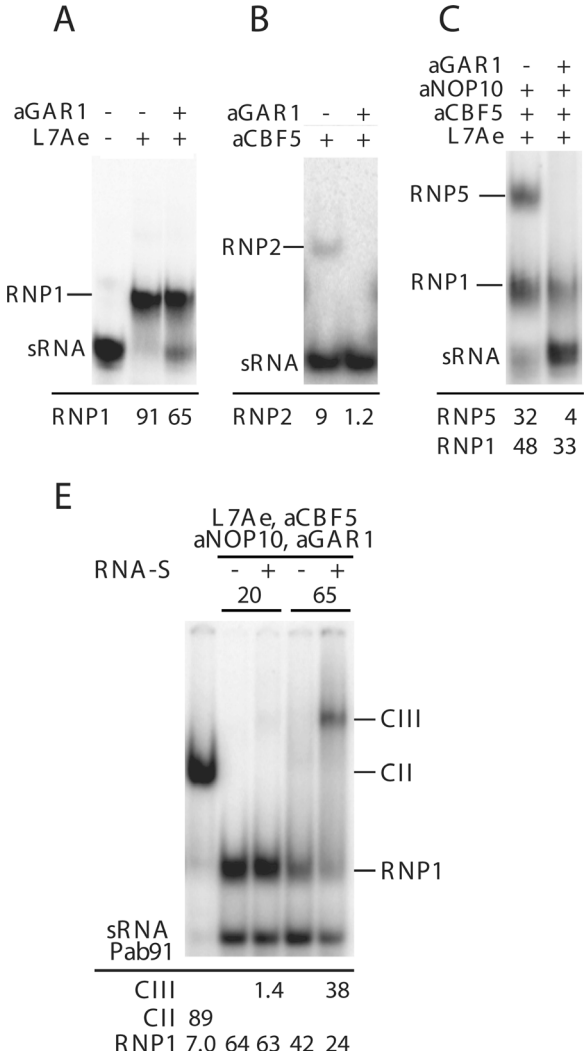

Figure 6. A decreased yield of RNP1, RNP2 and RNP5 formation in the presence of protein aGAR1 is counteracted by RNA-S. (**A–C**) The radiolabeled Pab91 sRNA (50 fmol) was incubated at 65°C with individual proteins or protein combinations, as indicated above the panels, in the absence or the presence of protein aGAR1. All the proteins were used at a 200 nM concentration. The percentage of Pab91 sRNA in RNP1 (Panel A), RNP2 (Panel B), and RNP1 and RNP5 (Panel C), is given below the lanes. (**D**) Same experiment as in Figure 4C, lanes 6–9, with the L7Ae, aCBF5, aNOP10 and aGAR1 protein set, and RNA-S substrate when indicated on top of the lanes.

We hypothesized that the aGAR1 negative effect on sRNP formation may be due to the formation of an aCBF5–aGAR1 interaction that destabilized the aCBF5–aNOP10 interaction. To test this hypothesis, Glutathione-Sepharose beads were coated with the GST–aGAR1 fusion protein. As shown by SDS–PAGE analysis (Figure 3), protein aCBF5, but not aNOP10 or L7Ae were retained on the beads, showing a direct interaction between aCBF5 and aGAR1. In addition, aNOP10 was not retained on the beads even when incubated together with aCBF5. Thus, the detected aCBF5–aGAR1 interaction is probably exclusive of the aCBF5–aNOP10 interaction. Interestingly, however, the negative effect of aGAR1 on RNP formation was partially counteracted in the presence of the RNA target. This is evidenced by the formation of a highly retarded complex CIII upon incubation of RNA-S with the WT

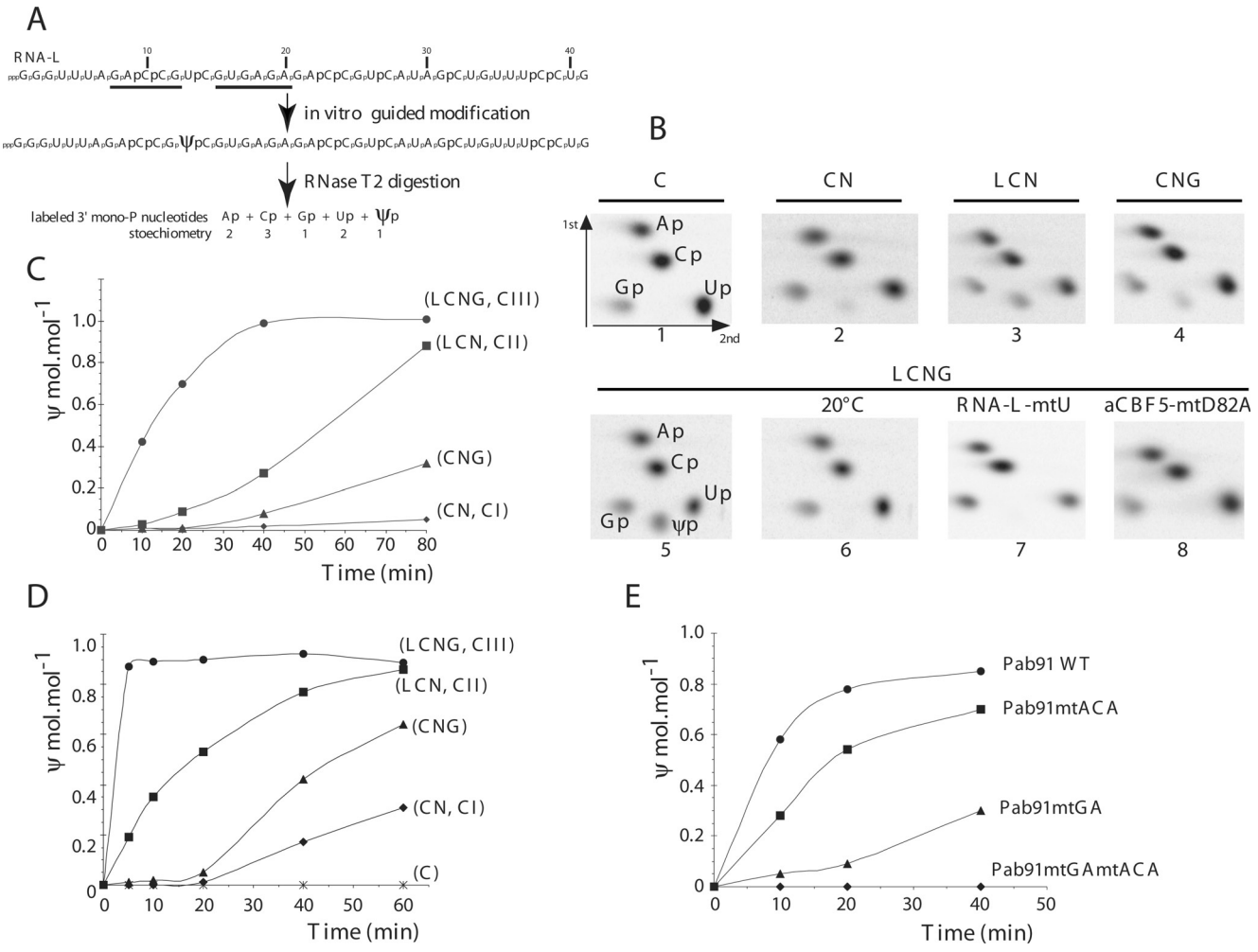

Figure 7. RNA-guided pseudouridylation of RNA target. (**A**) The 41 nt long RNA-L target used for analysis of RNP activity. Labeled phosphate after incorporation of [α-^{32}P]CTP are in bold. The sequence complementary to Pab91 sRNA is underlined. After T2 RNase digestion, residues U13p, U26p and U37p were labeled. Residue U13 is the expected pseudouridylation site (see also Figure 4A). (**B**) 2D-TLC analysis of Ψ formation. The RNA target (150 fmol) was mixed with 4 pmol of unlabeled WT sRNA and various combinations of the core proteins (200 nM each) and incubated for 80 min at 65°C (chromatograms 1–5 and 7–8), or 20°C (chromatogram 6). Incubation conditions are described in Materials and Methods. The following protein sets were used: aCBF5 alone (C), aCBF5 + aNOP10 (CN), L7Ae + aCBF5 + aNOP10 (LCN), aCBF5 + aNOP10 + aGAR1 (CNG), the complete set of core proteins (LCNG). In chromatogram 8, the variant aCBF5–mtD82A protein was used instead of the WT aCBF5 enzyme. After RNase T2 digestion and 2D TLC analysis, the Ap, Cp, Up, Gp and Ψp spots indicated in (B), were identified by comparison with reference maps (47). (**C**–**E**) Time course of the *in vitro* pseudouridylation reaction using the RNA-L (Panels C and E) or RNA-S (Panel D) target. The unlabeled WT or variant Pab91 sRNA was incubated with the various protein combinations (C, CN, LCN, CNG and LCNG). The amount of Ψ residue formed was estimated by 2D TLC for RNA-L and 1D TLC for RNA-S (see Figure S1, Supplementary Material).

guide RNA and the four core proteins (Figure 6D). The CIII electrophoretic mobility was markedly lower than that of complex CII. Interestingly, complex CIII was not detected at 20°C.

The *in vitro* assembled complex CIII is active in pseudouridylation

To test for the RNA:ψ-synthase activity of the reconstituted sRNP/RNA-S complexes, we used an approach based on the nearest-neighbor analysis (46). To get an idea of the specificity of the reaction, we used a 41 nt long RNA substrate (RNA-L) that carried a 3′ extension compared to RNA-S. This RNA contained several uridine residues in addition to the one targeted by the Pab91 sRNA (Figure 7A). We verified that the CI, CII and CIII series of complexes was obtained with RNA-L (data not shown). Then, a uniformly labeled RNA-L was produced by *in vitro* transcription in the presence of [α-^{32}P]CTP. After its digestion by RNase T2, three of the released 3′-monophosphate U residues were labeled, because they were followed by a C residue in the RNA molecule. One of them (U13) was the Pab91 sRNP target (Figure 6A). The labeled RNA-L was incubated 60 min with the WT Pab91 sRNA and the four core proteins in condition of complex CIII formation. Fractionation by thin layer chromatography of the nucleotides released upon T2 RNase digestion revealed a high yield of Ψ formation (Figure 7B). The experiment was repeated several times and for each experiment, the radioactivity of the fractionated 3′-monophosphate residues was measured with a phosphorimager. By taking into account the numbers of A, C, G and U residues followed by a C residue in RNA-L, we estimated the yield of U to Ψ conversion.

The mean value was found to be of 0.98 ± 0.05 mole of Ψ residue per mole of target RNA. In agreement with the idea that aCBF5 is the catalyst, no Ψ formation was detected when the aCBF5–D82A variant was used instead of the WT protein (Figure 7B). However, incubation of RNA-L with the aCBF5 protein alone was not sufficient for Ψ formation (Figure 7B). In agreement with the absence of complex CIII formation at 20°C (Figure 6D), Ψ formation only took place at an elevated temperature (Figure 7B). Pseudouridylation specifically occurred at the Pab91 targeted site, since after U to C substitution at this position no Ψ formation was detected (Figure 7B).

Some of the partially assembled H/ACA sRNPs also display specific RNA:Ψ-synthase activity

When the same test of activity was performed with the CI complex containing proteins aCBF5 and aNOP10, a very low level of Ψ formation was detected (0.08 ± 0.04 mol.mol^{-1}, mean value of three distinct experiments, Figure 7B and C). This low value was markedly increased (0.56 ± 0.08 mol·mol^{-1}), when the L7Ae protein was added to the incubation mixture (Figure 7B and C). Hence, the presence of protein L7Ae together with proteins aCBF5 and aNOP10 is sufficient for the formation of active particles. Whereas the activity of these particles was increased by addition of protein aGAR1, RNPs formed with the aCBF5, aNOP10 and aGAR1 protein combination were quite less efficient than RNPs assembled with the L7Ae, aCBF5 and aNOP10 protein set (mean value of 0.15 ± 0.07 mol·mol^{-1}, Figure 7B and C).

The short RNA-S substrate is more efficiently modified than the RNA-L substrate

We compared the kinetics of Ψ formation in both RNA-L and RNA-S (Figure 7C and D and Supplementary Material). In condition allowing complex CIII formation, one Ψ residue per mole of RNA-L was formed after 40 min of incubation. In the absence of aGAR1 (CII complex), a doubling of the incubation time was required to get the same level of modification (Figure 7C). In the presence of aGAR1 and the absence of L7Ae, only 30% of the RNA-L molecules were modified after 80 min of incubation and only trace amounts of modification were observed in the absence of both L7Ae and aGAR1 (CI complex). In contrast, when using the RNA-S substrate, a plateau of modification (90%) was reached after only 5 min of incubation in conditions of complex CIII formation. In the absence of protein aGAR1 (CII complex), the plateau was reached after 60 min of incubation. When the aCBF5–aNOP10–aGAR1 and aCBF5–aNOP10 protein combinations were used, 60 and 30% of the molecules were, respectively, modified after 60 min of incubation. Nevertheless, for both RNA substrates, a 20-min lag period was observed when protein L7Ae was not present in the reaction mixture. Hence, in the *in vitro* conditions that we used, both proteins L7Ae and aGAR1 increased the kinetics of the reaction.

Pseudouridylation by archaeal sRNP can occur in the absence of the ACA motif

As the Pab91mtGA and Pab91mtACA sRNA variants, respectively, formed CI-like and CII-like complexes with proteins L7Ae, aCBF5 and aNOP10 (Figure 4E), we tested whether these RNAs could guide RNA-L pseudouridylation in the presence of the four core proteins. As shown in Figure 7E, whereas the double Pab91mtGAmtACA mutant had no RNA guiding capacity, the Pab91mtGA and Pab91mtACA variants both allowed RNA-L pseudouridylation. In addition, after a 40-min incubation, the pseudouridylation activity of the Pab91mtACA sRNP was ~80% compared to that of the WT sRNP. Thus, the ACA motif is not essential for H/ACA sRNA activity *in vitro*.

DISCUSSION

Here for the first time, an active H/ACA RNP is obtained by incubation of its purified components. This is also the first study on archaeal H/ACA sRNP assembly. Up to now, only the H/ACA protein L7Ae had been produced *in vitro* and was shown to bind H/ACA sRNAs (25). By this reconstitution approach, we were able to dissect the relative roles of the four core proteins in H/ACA sRNP formation and activity. Our results bring important information on H/ACA RNPs in general and on the specificity of the archaeal system, compared to the eukaryal system.

The L7Ae–aCBF5–aNOP10–sRNA complex assembly in Archaea

In Eukarya, based on its very broad RNA specificity, protein NHP2/Nhp2p (L7Ae counterpart) was proposed to get its ability to recognize snoRNAs specifically upon incorporation into a GAR1–NAP57/CBF5–NOP10–NHP2 protein complex (36). This complex is formed in the cytoplasm, and then protein–snoRNA recognition takes place in the nucleus. The absence of cell compartmentalization in Archaea may explain the need for a more specific interaction of protein L7Ae with the H/ACA sRNAs. As expected, the pseudo K-turn motif of sRNA Pab91 is required for L7Ae binding. Interestingly, the aCBF5 RNA:Ψ-synthase also has an RNA binding capacity that is dependent on the presence of the ACA motif (Figure 1). However, even at high aCBF5 concentration, only a fraction of the sRNA molecules was bound to the protein (Figure 1C). One possible explanation is that aCBF5 does not form a stable complex with the Pab91 sRNA and dissociate during the electrophoresis. Alternatively, a small number of the sRNA molecules may have the conformation required for aCBF5 binding, or the aCBF5 proteins cleaved from the GST moiety have a limited solubility. As the yield of aCBF5 association was doubled in the presence of protein L7Ae (Figure 2A), L7Ae may either favor aCBF5 recruitment by protein–protein interaction or fold the sRNA in a more favorable conformation. No direct binding of the eukaryal NAP57/CBF5 protein on H/ACA snoRNAs was described, up to now. This, in spite of the presence in both the archaeal and eukaryal protein of a PUA domain supposed to bind RNA, and also of the greater size of the eukaryal NAP57/CBF5 proteins compared to archaeal proteins (42). In contrast, the aCBF5 and NAP57/CBF5 proteins have the common property to interact with proteins aNOP10 (Figure 3) and NOP10/Nop10p (35,36), respectively. Association of aNOP10 with the sRNA is strictly dependent on the presence of aCBF5 (Figure 2A). Protein L7Ae alone does not recruit aNOP10, although association of the aCBF5–aNOP10 complex protein pair with the

sRNA is markedly reinforced in the presence of protein L7Ae (Figure 2B). Hence, as found for the C/D box sRNPs (18,22), protein L7Ae likely plays an important role in H/ACA sRNP assembly. It may either reinforce the sRNA folding or interact with the aCBF5–aNOP10 pair. In favor of the latter hypothesis, an RNP5 complex containing the three proteins was formed on the Pab91mtACA variant, which is unable to bind protein aCBF5 alone. Nevertheless, the very low yield of RNP5 formation with this variant RNA and the absence of stable L7Ae–aCBF5–aNOP10 trimer detection by GST pull-down experiments (Figure 3), is not in favor of the formation of an L7Ae–aCBF5–aNOP10 complex prior association with the sRNA, as found in Eukarya (35,36).

Interestingly, our data show that the aCBF5–aNOP10–sRNA complex and to a greater extent the L7Ae–aCNF5–aNOP10–sRNA complex are stabilized in the presence of the RNA substrate (Figure 4). This suggests a higher affinity of the aCBF5–aNOP10 heterodimer and L7Ae–aCBF5–aNOP10 heterotrimer for the RNA structure formed after base-pair interaction of the substrate RNA with the sRNA than for the free sRNA.

The L7Ae–aCBF5–aNOP10–sRNA complex is active in pseudouridylation

The small amount of RNP2 complex, formed by protein aCBF5 alone, had no detectable RNA:Ψ-synthase activity. The minimal set of proteins needed to detect activity is the aCBF5–aNOP10 pair (Figure 7), which is in agreement with the requirement of aNOP10 for efficient binding of the RNA substrate (Figure 4C). Protein aNOP10 has probably the capability to stabilize the guide RNA/target RNA interaction. The fact that the RNA substrate association strongly depends upon the presence of the targeted U residue (Figure 5) reinforces the idea of a needed RNA–protein interaction for stable association of the RNA substrate. It also indicates that the possibility to form the bipartite helices in the pseudouridylation pocket is not sufficient for a stable docking of the RNA substrate on the sRNP.

Although measurable, the activity observed with the two aCBF5 and aNOP10 proteins was low. The aCBF5–aNOP10–aGAR1 protein triplet was slightly more efficient (Figure 7). However, the L7Ae–aCBF5–aNOP10 protein triplet was quite more efficient. This reinforced efficiency may be linked to the positive effect of protein L7Ae on association of the aCBF5–aNOP10 pair. Accordingly, for both RNA-L and RNA-S substrates, a 20-min lag period without detectable RNA:Ψ-synthase activity was observed in the absence of protein L7Ae. This lag period may be needed to get an efficient aCBF5–aNOP10 recruitment in the absence of protein L7Ae. Accordingly, the same lag period is observed with the Pab91mtGA sRNA mutated in the L7Ae binding site.

aGAR1 increases the pseudouridylation efficiency of the Pab91 sRNP complexes

We are facing two puzzling observations. On the one hand, except for RNP1, the yield of RNP formation in the absence of RNA substrate is strongly reduced in the presence of protein aGAR1 (Figure 6). On the other hand, addition of protein aGAR1 increases the yield of substrate pseudouridylation at a given time point (Figure 7). Importantly also, in the presence of the RNA substrate, the four proteins form a stable CIII complex (Figure 6E). This suggests that in the *in vitro* conditions used, the sRNP core protein complex is only stable in the presence of the RNA substrate. Furthermore, whereas aCBF5–aGAR1 and aCBF5–aNOP10 interactions were detected in our GST pull-down experiments, we did not detect a stable aCBF5–aNOP10–aGAR1 triple interaction. This may be due to the presence of the GST tag on the proteins. However, an exclusive interaction of the free aCBF5 protein with either aNOP10 or aGAR1 is in agreement with the data listed above. Triple interaction may be stable only in presence of both the sRNA and the target RNA. In light of the strong differences observed between the archaeal and eukaryal sRNP assembly, it should be pointed out that proteins L7Ae and Nhp2p/NHP2 have different behaviors. Whereas L7Ae binds strongly and specifically to the sRNA and may be the first protein bound to the sRNA, protein Nhp2p/NHP2 has poor and non specific RNA binding properties (48). It probably gains its specific RNA binding property in association with the other proteins in the aCBF5–aNOP10–NHP2 heterotrimer or in the aCBF5–aNOP10–aGAR1–NHP2 heterotetramer (36). Difference between the eukaryal and archaeal systems may essentially concern the sRNP and snoRNP assembly pathways. Observation by crosslink experiments of the location of protein GAR1 near the catalytic center is consistent with a possible interaction with the RNA substrate and with its possible involvement in the catalytic reaction. The enhancement of the yield of pseudouridylation that we observed in the presence of protein aGAR1 (Figure 7) suggests that this protein increases the catalytic efficiency of the particles: it may either favor a conformational transition leading to active sRNP particles or increase the kinetics of dissociation after the reaction. Further experiments are underway to test for these alternative explanations. Indeed, due to our utilization of an excess of RNP components compared to RNA substrate (molar excess of sRNA compared to RNA target of 26), we have no information on the turnover of the reaction. Nevertheless, this point will be important to address, since no ATP-dependent RNA helicase activity is used in the *in vitro* system, although the interaction formed by the guide Pab91 sRNA and its RNA substrate has a high free energy (−17.7 kcal/mol). Remarkably, as a C instead of a U at the pseudouridylation position had a strong negative effect on substrate assembly (Figure 5), destabilization of the target RNA may simply be due to Ψ formation.

In conclusion, we report here the successful development of an efficient *in vitro* pseudouridylation system that is based on the use of recombinant archaeal components. The advantage of this system compared to the eukaryal system is the great solubility of the archeal H/ACA core proteins. The assembly conditions developed will facilitate further studies on H/ACA sRNP structure and function. In addition, they represent a very useful tool for the *in vitro* generation of a Ψ residue at defined positions in RNAs.

Note

After we submitted this manuscript, Baker *et al*. reported in *Genes Dev*., the reconstitution and activity of H/ACA sRNP particles by using the proteins and a modified Pf9 H/ACA guide sRNA from *Pyrococcus furiosus*.

SUPPLEMENTARY MATERIAL

Supplementary Material is available at NAR Online.

ACKNOWLEDGEMENTS

We thank Dr Hannu Myllykallio (P. Forterre Lab) for his gift of *P.abyssi* genomic DNA. F. Leclerc is thanked for providing information on H/ACA sRNAs before publication. S. Massenet and Y. Motorin are thanked for their critical reading of the manuscript. The work was supported by the Centre National de la Recherche Scientifique (CNRS), the French Ministère de la Recherche et des Nouvelles Technologies (MRNT), the Actions Concertées Incitatives (ACI) Microbiologie and BCMS of the french MRNT and the Bioingénierie PRST of the Conseil Régional Lorrain. Funding to pay the Open Access publication charges for this article was provided by the Service Commun de Documentation de l' UHP-Nancy I.

Conflict of interest statement. None declared.

REFERENCES

1. Decatur,W.A. and Fournier,M.J. (2003) RNA-guided nucleotide modification of ribosomal and other RNAs. *J. Biol. Chem.*, **278**, 695–698.
2. Massenet,S., Mougin,A. and Branlant,C. (1998) Posttranscriptional modifications in the U small nuclear RNAs. In Grosjean,H. and Benne,R. (eds), *The Modification and Editing of RNA*. ASM Press, New York, pp. 201–227.
3. Bonnerot,C., Pintard,L. and Lutfalla,G. (2003) Functional redundancy of Spb1p and a snR52-dependent mechanism for the 2′-O-ribose methylation of a conserved rRNA position in yeast. *Mol. Cell*, **12**, 1309–1315.
4. Donmez,G., Hartmuth,K. and Luhrmann,R. (2004) Modified nucleotides at the 5′ end of human U2 snRNA are required for spliceosomal E-complex formation. *RNA*, **10**, 1925–1933.
5. King,T.H., Liu,B., McCully,R.R. and Fournier,M.J. (2003) Ribosome structure and activity are altered in cells lacking snoRNPs that form pseudouridines in the peptidyl transferase center. *Mol. Cell*, **11**, 425–435.
6. Lapeyre,B. and Purushothaman,S.K. (2004) Spb1p-directed formation of Gm2922 in the ribosome catalytic center occurs at a late processing stage. *Mol. Cell*, **16**, 663–669.
7. Yang,C., McPheeters,D.S. and Yu,Y.T. (2005) psi 35 in the branch site recognition region of U2 snRNA is important for pre-mRNA splicing in *S. cerevisiae*. *J. Biol. Chem.*, **280**, 6655–6662.
8. Ansmant,I. and Motorin,I. (2001) Identification of RNA modification enzymes using sequence homology. *Mol. Biol. (Mosk.)*, **35**, 248–267.
9. Ofengand,J. (2002) Ribosomal RNA pseudouridines and pseudouridine synthases. *FEBS Lett.*, **514**, 17–25.
10. Omer,A.D., Ziesche,S., Decatur,W.A., Fournier,M.J. and Dennis,P.P. (2003) RNA-modifying machines in archaea. *Mol. Microbiol.*, **48**, 617–629.
11. Bachellerie,J.P., Cavaille,J. and Huttenhofer,A. (2002) The expanding snoRNA world. *Biochimie*, **84**, 775–790.
12. Terns,M.P. and Terns,R.M. (2002) Small nucleolar RNAs: versatile *trans*-acting molecules of ancient evolutionary origin. *Gene Expr.*, **10**, 17–39.
13. Kiss,T. (2002) Small nucleolar RNAs: an abundant group of noncoding RNAs with diverse cellular functions. *Cell*, **109**, 145–148.
14. Kiss-Laszlo,Z., Henry,Y. and Kiss,T. (1998) Sequence and structural elements of methylation guide snoRNAs essential for site-specific ribose methylation of pre-rRNA. *EMBO J.*, **17**, 797–807.
15. Omer,A.D., Lowe,T.M., Russell,A.G., Ebhardt,H., Eddy,S.R. and Dennis,P.P. (2000) Homologs of small nucleolar RNAs in Archaea. *Science*, **288**, 517–522.
16. Ganot,P., Caizergues-Ferrer,M. and Kiss,T. (1997) The family of box ACA small nucleolar RNAs is defined by an evolutionarily conserved secondary structure and ubiquitous sequence elements essential for RNA accumulation. *Genes Dev.*, **11**, 941–956.
17. Ni,J., Tien,A.L. and Fournier,M.J. (1997) Small nucleolar RNAs direct site-specific synthesis of pseudouridine in ribosomal RNA. *Cell*, **89**, 565–573.
18. Omer,A.D., Ziesche,S., Ebhardt,H. and Dennis,P.P. (2002) *In vitro* reconstitution and activity of a C/D box methylation guide ribonucleoprotein complex. *Proc. Natl. Acad. Sci. USA*, **99**, 5289–5294.
19. Tran,E., Brown,J. and Maxwell,E.S. (2004) Evolutionary origins of the RNA-guided nucleotide-modification complexes: from the primitive translation apparatus? *Trends Biochem. Sci.*, **29**, 343–350.
20. Watkins,N.J., Segault,V., Charpentier,B., Nottrott,S., Fabrizio,P., Bachi,A., Wilm,M., Rosbash,M., Branlant,C. and Luhrmann,R. (2000) A common core RNP structure shared between the small nucleolar box C/D RNPs and the spliceosomal U4 snRNP. *Cell*, **103**, 457–466.
21. Bortolin,M.L., Bachellerie,J.P. and Clouet-d'Orval,B. (2003) *In vitro* RNP assembly and methylation guide activity of an unusual box C/D RNA, *cis*-acting archaeal pre-tRNA(Trp). *Nucleic Acids Res.*, **31**, 6524–6535.
22. Tran,E.J., Zhang,X. and Maxwell,E.S. (2003) Efficient RNA 2′-O-methylation requires juxtaposed and symmetrically assembled archaeal box C/D and C'/D' RNPs. *EMBO J.*, **22**, 3930–3940.
23. Rashid,R., Aittaleb,M., Chen,Q., Spiegel,K., Demeler,B. and Li,H. (2003) Functional requirement for symmetric assembly of archaeal box C/D small ribonucleoprotein particles. *J. Mol. Biol.*, **333**, 295–306.
24. Singh,S.K., Gurha,P., Tran,E.J., Maxwell,E.S. and Gupta,R. (2004) Sequential 2′-O-methylation of archaeal pre-tRNATrp nucleotides is guided by the intron-encoded but trans-Acting Box C/D Ribonucleoprotein of Pre-tRNA. *J. Biol. Chem.*, **279**, 47661–47671.
25. Rozhdestvensky,T.S., Tang,T.H., Tchirkova,I.V., Brosius,J., Bachellerie,J.P. and Huttenhofer,A. (2003) Binding of L7Ae protein to the K-turn of archaeal snoRNAs: a shared RNA binding motif for C/D and H/ACA box snoRNAs in Archaea. *Nucleic Acids Res.*, **31**, 869–877.
26. Balakin,A.G., Smith,L. and Fournier,M.J. (1996) The RNA world of the nucleolus: two major families of small RNAs defined by different box elements with related functions. *Cell*, **86**, 823–834.
27. Bortolin,M.L., Ganot,P. and Kiss,T. (1999) Elements essential for accumulation and function of small nucleolar RNAs directing site-specific pseudouridylation of ribosomal RNAs. *EMBO J.*, **18**, 457–469.
28. Ganot,P., Bortolin,M.L. and Kiss,T. (1997) Site-specific pseudouridine formation in preribosomal RNA is guided by small nucleolar RNAs. *Cell*, **89**, 799–809.
29. Heiss,N.S., Girod,A., Salowsky,R., Wiemann,S., Pepperkok,R. and Poustka,A. (1999) Dyskerin localizes to the nucleolus and its mislocalization is unlikely to play a role in the pathogenesis of dyskeratosis congenita. *Hum. Mol. Genet.*, **8**, 2515–2524.
30. Lafontaine,D.L., Bousquet-Antonelli,C., Henry,Y., Caizergues-Ferrer,M. and Tollervey,D. (1998) The box H ACA snoRNAs carry Cbf5p, the putative rRNA pseudouridine synthase. *Genes Dev.*, **12**, 527–537.
31. Meier,U.T. and Blobel,G. (1994) NAP57, a mammalian nucleolar protein with a putative homolog in yeast and bacteria. *J. Cell Biol.*, **127**, 1505–1514.
32. Watkins,N.J., Gottschalk,A., Neubauer,G., Kastner,B., Fabrizio,P., Mann,M. and Luhrmann,R. (1998) Cbf5p, a potential pseudouridine synthase, and Nhp2p, a putative RNA-binding protein, are present together with Gar1p in all H BOX/ACA-motif snoRNPs and constitute a common bipartite structure. *RNA*, **4**, 1549–1568.
33. Henras,A., Henry,Y., Bousquet-Antonelli,C., Noaillac-Depeyre,J., Gelugne,J.P. and Caizergues-Ferrer,M. (1998) Nhp2p and Nop10p are essential for the function of H/ACA snoRNPs. *EMBO J.*, **17**, 7078–7090.
34. Wang,C., Query,C.C. and Meier,U.T. (2002) Immunopurified small nucleolar ribonucleoprotein particles pseudouridylate rRNA independently of their association with phosphorylated Nopp140. *Mol. Cell Biol.*, **22**, 8457–8466.
35. Henras,A.K., Capeyrou,R., Henry,Y. and Caizergues-Ferrer,M. (2004) Cbf5p, the putative pseudouridine synthase of H/ACA-type snoRNPs, can form a complex with Gar1p and Nop10p in absence of Nhp2p and box H/ACA snoRNAs. *RNA*, **10**, 1704–1712.
36. Wang,C. and Meier,U.T. (2004) Architecture and assembly of mammalian H/ACA small nucleolar and telomerase ribonucleoproteins. *EMBO J.*, **23**, 1857–1867.

37. Dragon,F., Pogacic,V. and Filipowicz,W. (2000) *In vitro* assembly of human H/ACA small nucleolar RNPs reveals unique features of U17 and telomerase RNAs. *Mol. Cell Biol.*, **20**, 3037–3048.
38. Pogacic,V., Dragon,F. and Filipowicz,W. (2000) Human H/ACA small nucleolar RNPs and telomerase share evolutionarily conserved proteins NHP2 and NOP10. *Mol. Cell Biol.*, **20**, 9028–9040.
39. Tang,T.H., Bachellerie,J.P., Rozhdestvensky,T., Bortolin,M.L., Huber,H., Drungowski,M., Elge,T., Brosius,J. and Huttenhofer,A. (2002) Identification of 86 candidates for small non-messenger RNAs from the archaeon *Archaeoglobus fulgidus*. *Proc. Natl Acad. Sci. USA*, **99**, 7536–7541.
40. Hamma,T. and Ferre-D'Amare,A.R. (2004) Structure of protein L7Ae bound to a K-turn derived from an archaeal box H/ACA sRNA at 1.8 A resolution. *Structure (Camb.)*, **12**, 893–903.
41. Charron,C., Manival,X., Clery,A., Senty-Segault,V., Charpentier,B., Marmier-Gourrier,N., Branlant,C. and Aubry,A. (2004) The archaeal sRNA binding protein L7Ae has a 3D structure very similar to that of its eukaryal counterpart while having a broader RNA-binding specificity. *J. Mol. Biol.*, **342**, 757–773.
42. Watanabe,Y. and Gray,M.W. (2000) Evolutionary appearance of genes encoding proteins associated with box H/ACA snoRNAs: cbf5p in *Euglena gracilis*, an early diverging eukaryote, and candidate Gar1p and Nop10p homologs in archaebacteria. *Nucleic Acids Res.*, **28**, 2342–2352.
43. Charron,C., Manival,X., Charpentier,B., Branlant,C. and Aubry,A. (2004) Purification, crystallization and preliminary X-ray diffraction data of L7Ae sRNP core protein from *Pyrococcus abyssi*. *Acta Crystallogr. D. Biol. Crystallogr.*, **60**, 122–124.
44. Marmier-Gourrier,N., Clery,A., Senty-Segault,V., Charpentier,B., Schlotter,F., Leclerc,F., Fournier,R. and Branlant,C. (2003) A structural, phylogenetic, and functional study of 15.5-kD/Snu13 protein binding on U3 small nucleolar RNA. *RNA*, **9**, 821–838.
45. Mougin,A., Gregoire,A., Banroques,J., Segault,V., Fournier,R., Brule,F., Chevrier-Miller,M. and Branlant,C. (1996) Secondary structure of the yeast *Saccharomyces cerevisiae* pre-U3A snoRNA and its implication for splicing efficiency. *RNA*, **2**, 1079–1093.
46. Motorin,Y., Keith,G., Simon,C., Foiret,D., Simos,G., Hurt,E. and Grosjean,H. (1998) The yeast tRNA:pseudouridine synthase Pus1p displays a multisite substrate specificity. *RNA*, **4**, 856–869.
47. Keith,G. (1995) Mobilities of modified ribonucleotides on two-dimensional cellulose thin-layer chromatography. *Biochimie*, **77**, 142–144.
48. Henras,A., Dez,C., Noaillac-Depeyre,J., Henry,Y. and Caizergues-Ferrer,M. (2001) Accumulation of H/ACA snoRNPs depends on the integrity of the conserved central domain of the RNA-binding protein Nhp2p. *Nucleic Acids Res.*, **29**, 2733–2746.